Biosensors

Controlling Lipid Membrane Architecture for Tunable Nanoplasmonic Biosensing

*Goh Haw Zan, Joshua A. Jackman, Seong-Oh Kim, and Nam-Joon Cho**

We report the development of lipid membrane platforms with a tunable measurement response for nanoplasmonic biosensing applications. Three types of lipid membrane platforms, including a planar lipid bilayer, adsorbed vesicle layer, and vesicle islands surrounded by a planar bilayer, were formed on coated gold nanodisk arrays via material-selective self-assembly. The interaction between a membrane-active peptide and the lipid membrane platforms was strongly influenced by membrane architecture, and the corresponding measurement response was sensitive to the lipid environment surrounding the gold nanodisks. In combination with time derivative analysis, the findings delineate how nanoplasmonic biosensing of biologically relevant interactions can be optimized via controlling lipid membrane architecture.

Localized surface plasmon resonance (LSPR) of metallic and semiconducting nanoparticles provides a highly surface-sensitive transducing element to detect perturbations in the refractive index of the local environment.[1–3] Based on the resonance of coherently oscillating conduction band electrons excited by light, nanoplasmonic sensing benefits from a short penetration (sensing) depth, fast response, high sensitivity, indefinite measurement lifetime, simple technical requirements, and flexible experimental design. Depending on a nanoparticle's size and shape, there is a characteristic extinction wavelength maximum, λ_{max}, which shifts according to changes in the local dielectric environment. In biosensor applications (e.g., protein binding), the measurement response is typically a redshift in the extinction spectrum because most organic molecules have a higher refractive index than buffer solution.

With the continued growth in nanoplasmonic biosensing applications for nucleic acids, peptides, and proteins, there is strong interest to develop nanoplasmonic sensing platforms for lipid membrane applications.[4,5] Thus far, several types of nanoplasmonic sensing platforms have been applied to study lipid membranes, with particular emphasis on platform fabrication of structurally homogenous membranes (e.g., supported lipid bilayers or so-called SLBs) and tracking of simple ligand-receptor binding events (e.g., biotin-streptavidin). Early work by Dahlin *et al.* reported the self-assembly formation of phospholipid assemblies, including an SLB[6] and single tethered lipid vesicles,[7] within nanometric holes on a thin gold film. SLB formation via vesicle adsorption and rupture on silicon oxide-coated, nanohole-containing gold and silver films was also reported[8,9] and noteworthy because it represented the first example of a structural change detected by nanoplasmonic sensing at the biomacromolecular level. Additional research has mainly focused on protein binding to lipid bilayer-coated gold nanorods[10] and silver nanocubes,[11,12] as well as formation of SLBs on different plasmonic structures, including on top of nanodisks[13] and on topographically flat substrates with embedded nanodisks.[14]

Given the extensive literature pertaining to how surface-adsorbed lipids self-assemble into different membrane architectures depending on material characteristics (e.g., composition[15] and topography[16]), there exists ample opportunity to combine nanofabrication and molecular self-assembly in order to further advance nanoplasmonic sensing platforms for lipid membrane studies. Recently, an indirect nanoplasmonic sensing platform was described which comprises a random array of noninteracting gold nanodisks on a glass substrate.[17] The platform is formed via hole-mask colloidal lithography[18] and can be covered by a thin coat of a dielectric material. The dipole field from the LSPR

Dr. G. H. Zan, J. A. Jackman, S.-O. Kim, Prof. N.-J. Cho
School of Materials Science and Engineering
Nanyang Technological University
50 Nanyang Avenue, 639798, Singapore
E-mail: njcho@ntu.edu.sg
Dr. G. H. Zan, J. A. Jackman, S.-O. Kim, Prof. N.-J. Cho
Centre for Biomimetic Sensor Science
Nanyang Technological University
50 Nanyang Drive, 637553, Singapore
Prof. N.-J. Cho
School of Chemical and Biomedical Engineering
Nanyang Technological University
62 Nanyang Drive, 637459, Singapore

DOI: 10.1002/smll.201400518

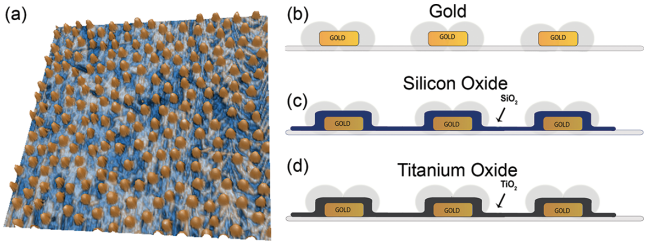

Scheme 1. Nanoplasmonic Sensing Platforms for Material-Selective Self-Assembly of Lipid Membranes. (a) AFM imaging of bare gold nanodisks on glass surface. The image size is 5 μm × 5 μm. The nanoplasmonic biosensing experiments were performed on (b) bare gold nanodisks on glass surface, (c) silicon oxide-coated nanodisk surface, and (d) titanium oxide-coated nanodisk surface.

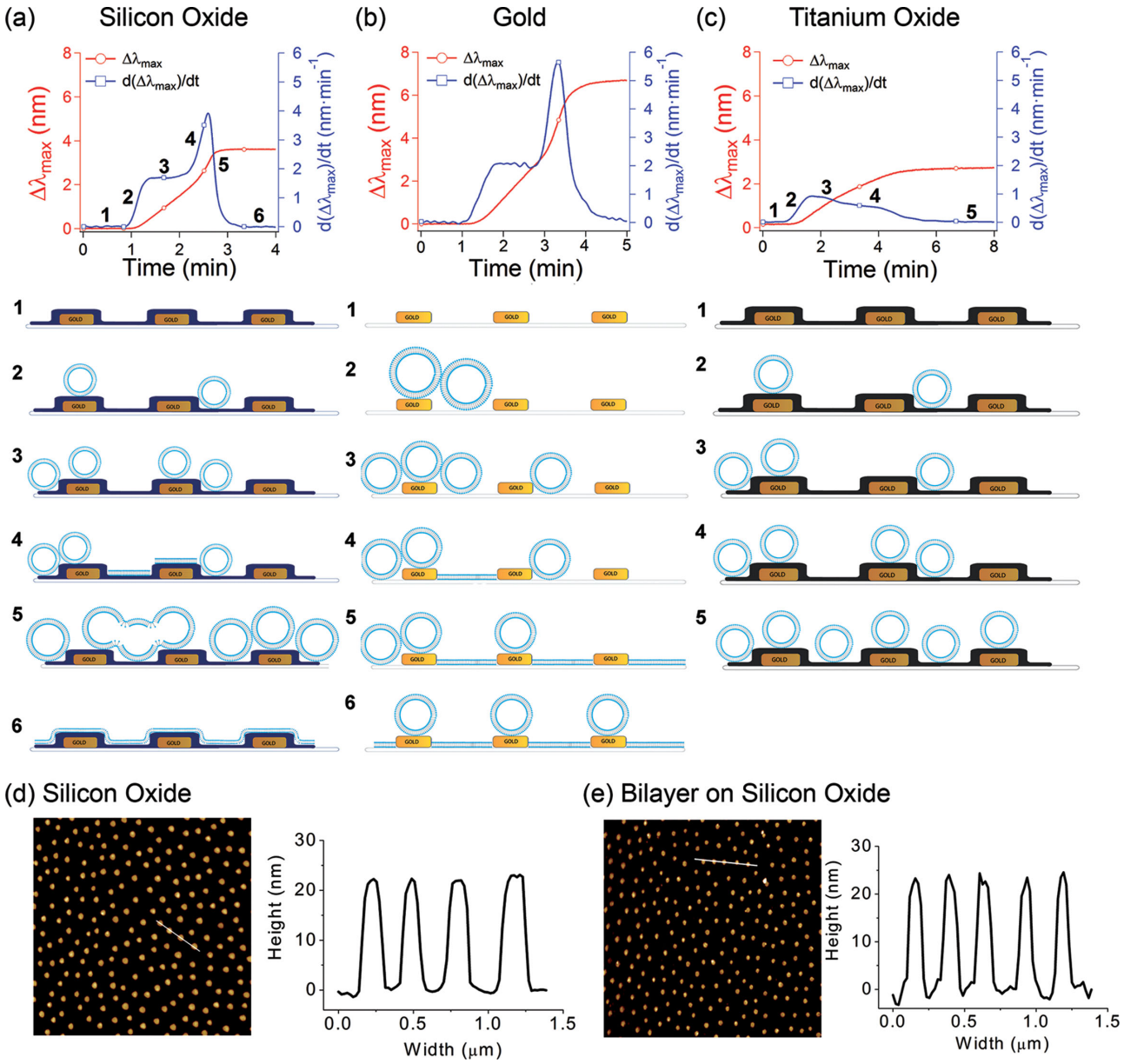

Figure 1. Self-Assembly Formation of Lipid Membranes on Nanoplasmonic Sensor Platforms. Time-resolved extinction maximum wavelength shift measurements (red) and corresponding time derivative (blue) for vesicle adsorption onto (a) silicon oxide-coated nanodisk surface, (b) bare gold nanodisks on glass surface, and (c) titanium oxide-coated nanodisk surface. The baseline measurement was recorded in aqueous buffer solution (10 mM Tris, 200 mM NaCl, pH 7.0), followed by vesicle addition after one minute. AFM imaging for silicon oxide-coated sensor platform (d) before and (e) after SLB formation. The image sizes are 5 μm × 5 μm.

penetrates the coating in order to monitor processes which occur on the film surface, including catalysis on platinum,[19] corrosion on copper,[20] and biomacromolecular adsorption on silicon oxide.[13] Herein, we investigated how the material-selective self-assembly of lipid membranes could be exploited for development of sensing platforms to track membrane-peptide interactions. Indeed, a key advantage of indirect nanoplasmonic sensing is control over the material composition of the surface coating.

Taking into account the dependence of lipid membrane formation on the surface coating, three different platforms were employed (**Scheme 1**). The template platform was a low density array of gold nanodisks deposited on a glass substrate. The nanodisks were highly uniform, with respect to diameter (100 ± 10 nm) and height (20 ± 1 nm). Two other platforms were fabricated by depositing a thin layer (~10 nm) of silicon oxide or titanium oxide on top of the gold nanodisks. The bare gold nanodisks on glass had more than two times greater measurement sensitivity than the coated substrates (232 nm/RIU vs. ca. 110 nm/RIU) (see Supporting Information, Figure S1).

Formation of lipid membranes on the nanoplasmonic sensing platforms occurred via vesicle adsorption. Depending on the material substrate and lipid composition, vesicle adsorption can follow different self-assembly pathways, including vesicle rupture to form an SLB (e.g., zwitterionic

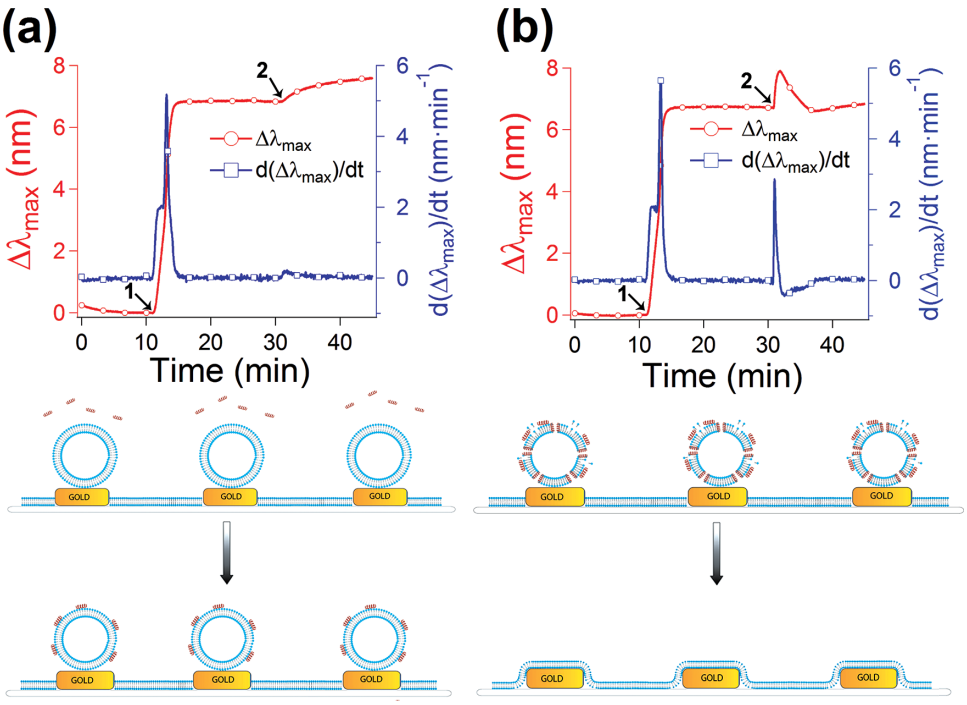

Figure 2. Membrane Curvature-Sensing of Amphipathic Peptide Binding to Vesicle Platforms. Time-resolved extinction maximum wavelength shift measurements (red) and corresponding time derivative (blue) for membrane-peptide interaction analysis. After vesicle addition onto bare gold nanodisks on glass surface (Arrow 1), either (a) 0.2 μM or (b) 13 μM peptide was then added (Arrow 2).

lipid vesicles on glass and silicon oxide) or remain as intact, adsorbed vesicles (e.g., zwitterionic lipid vesicles on gold and titanium oxide).[21] Small unilamellar vesicles (SUVs) composed of 1-palmitoyl-2-oleoyl-*sn*-glycero-3-phosphocholine were prepared by the extrusion method[22] (average diameter below 60 nm). To track vesicle adsorption, time-resolved extinction maximum shift measurements were performed in optical transmission mode. On silicon oxide, SLB formation was observed, as indicated by a characteristic acceleration in the extinction maximum shift shift response[8] (**Figure 1**a, red curve). In order to resolve the kinetics of bilayer formation in detail, the time derivative was also plotted to reveal a sequence as follows: 1) baseline in aqueous buffer; 2) onset of vesicle adsorption; 3) diffusion-limited vesicle adsorption; 4) vesicle rupture (starting from the critical vesicle surface coverage); 5) bilayer propagation; and 6) complete bilayer formation (Figure 1a, blue curve). Atomic force microscopy (AFM) experiments confirmed vesicle rupture (Figure 1d and e). A similar LSPR measurement response indicating SLB formation was also observed on bare gold nanodisks on glass (Figure 1b). This finding supports that a bilayer is formed, although the extent of SLB formation is unclear, including whether or not bilayers are formed on top of the gold nanodisks. By contrast, vesicle rupture did not occur on titanium oxide, thereby supporting formation of an adsorbed vesicle layer (Figure 1c). Compared to the previous two cases, deceleration of the LSPR measurement response on titanium oxide indicates that, as the surface coverage of adsorbed vesicles became more appreciable, the rate of adsorption decreased until finally reaching saturation coverage. In this case, the time derivative plot showed the following sequence: 1) baseline in aqueous buffer; 2) onset of vesicle adsorption; 3) diffusion-limited vesicle adsorption; 4) gradually reduced adsorption (due to increasing vesicle surface coverage); and 5) vesicle saturation. Overall, the collective set of kinetic data identifies the material-selective self-assembly of lipid membranes on the sensor coatings.

To next determine if adsorbed vesicles remain intact on top of the bare gold nanodisks on glass, we added a membrane curvature-sensing peptide that binds appreciably to highly curved membranes, but not to planar SLBs.[23,24] Addition of 200 nM peptide led to a monotonic increase in the LSPR measurement response, with a final $\Delta\lambda_{max}$ of 0.8 nm that corresponds to peptide binding (**Figure 2**a). Interestingly, there was essentially no measurement response to peptide binding in the time derivative plot. As a control experiment, 13 μM peptide was added to an SLB on silicon oxide, leading to a final $\Delta\lambda_{max}$ of only 0.1 nm (see Supporting Information, Figure S2). This evidence strongly supports there are intact vesicles remaining on the bare gold nanodisks on the basis of membrane curvature-sensing. 13 μM peptide was then added to lipid structures on the bare gold nanodisks (Figure 2b). A large increase in $\Delta\lambda_{max}$ of 1.2 nm was initially observed before decreasing again. The final $\Delta\lambda_{max}$ was only 0.1 nm, likely because the edges of the nanodisks are already covered by lipid bilayer. There was also a sharp corresponding peak in the time derivative plot, which indicates that the membrane-peptide interaction is more complex than simple peptide binding. Consistent with a previous report on peptide-induced rupture of surface-adsorbed vesicles on gold,[23] it appears that sufficiently high concentrations of the peptide rupture adsorbed vesicles to form an SLB on top of the gold nanodisks. Hence, these findings demonstrate that there are intact vesicles remaining on the bare gold nanodisks, and

NANO MICRO small

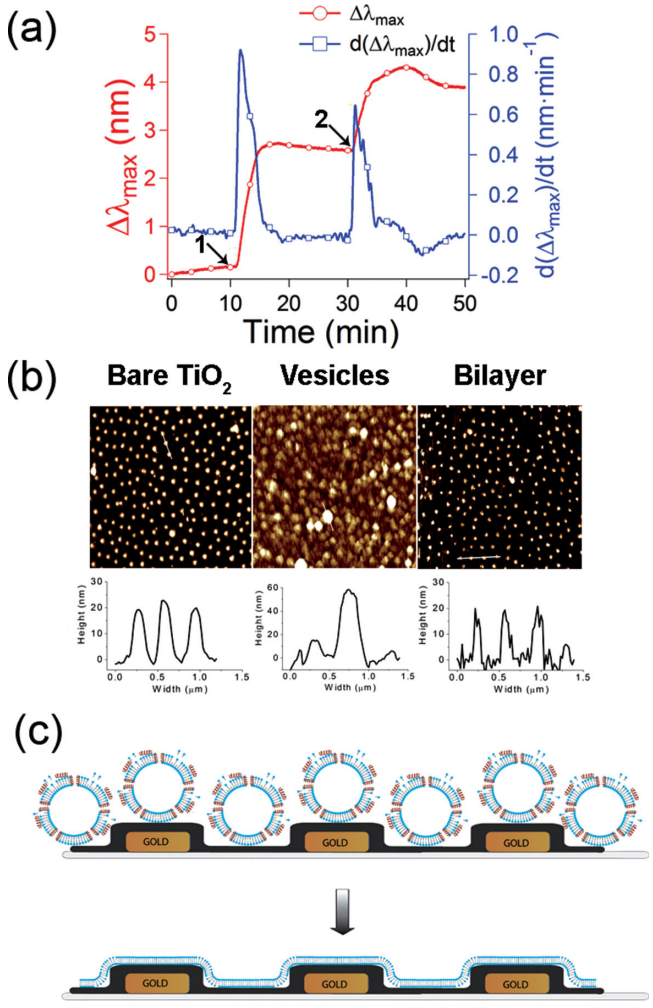

Figure 3. Peptide-Induced Rupture of Adsorbed Vesicles on Titanium Oxide. (a) Time-resolved extinction maximum wavelength shift measurements (red) and corresponding time derivative (blue). After vesicle addition onto the titanium oxide-coated sensing platform (Arrow 1), 13 μM peptide was then added (Arrow 2). (b) AFM imaging for (left) bare titanium oxide-coated sensor platform, (center) after vesicle addition, and (right) after peptide-induced SLB formation. The image sizes are 5 μm × 5 μm. (c) Scheme of peptide-induced vesicle rupture to form an SLB on titanium oxide-coated sensing platform.

that nanoplasmonic sensing can track the kinetics of peptide binding and peptide-induced vesicle rupture.

To compare peptide-induced vesicle rupture on lipid membrane platforms with different membrane architectures, 13 μM peptide was also added to the adsorbed vesicle layer on titanium oxide (**Figure 3**a). A large increase in $\Delta\lambda_{max}$ of 1.7 nm was again observed initially, followed by a decrease in the extinction maximum shift. By comparing the extinction maximum shift corresponding to maximum peptide binding before vesicle rupture on the bare gold and titanium oxide-coated nanodisks, respectively, it is observed that the measurement response on titanium oxide is appreciably localized on top of the nanodisk (~35%). The final $\Delta\lambda_{max}$ was 1.3 nm, which is more than 27 times greater than the measurement response on the bare gold nanodisk surface when accounting for the difference in measurement sensitivity. On titanium oxide, it therefore appears that the peptide induces rupture of adsorbed vesicles across the entire platform, as confirmed by AFM measurements (Figure 3b). The final $\Delta\lambda_{max}$ associated with peptide-induced vesicle rupture on titanium oxide is largely related to the vesicle-to-bilayer structural transformation that occurs in the lipid environment surrounding the gold nanodisk (Figure 3c). By contrast, no such transformation occurred on the bare gold nanodisks because the surrounding environment already has a planar SLB on glass. Taken together, the peptide-induced vesicle experiments on bare or titanium oxide-coated gold nanodisks demonstrate that the nanoplasmonic measurement response is sensitive to the surrounding lipid environment, thereby offering a design strategy to control membrane architecture as evidenced herein by material-selective self-assembly.

In conclusion, we have demonstrated the material-selective fabrication of lipid membrane platforms for nanoplasmonic biosensing applications. Depending on the material coating, a planar lipid bilayer, adsorbed vesicle layer, or vesicle arrays surrounded by a planar bilayer was formed. Membrane curvature-selective binding of a peptide was detected at low peptide concentration, whereas the same peptide caused vesicle rupture at appreciably higher peptide concentration. Importantly, the LSPR measurement response of peptide-induced vesicle rupture varied in a manner which is consistent with the surrounding lipid environment. This capability opens the door to tuning the measurement response based on lipid membrane architecture, which strongly complements additional material-inspired (e.g., synergestically modulating inter-particle and substrate-particle interactions[25]) and biologically-inspired (e.g., programmable DNA-mediated assembly of plasmonic metamaterials[26]) strategies. Furthermore, compared to previously reported nanoplasmonic sensing platforms that employ single vesicles in nanowells[7] and nanomehirs,[27] the platforms described herein do not require covalent tethering or surface passivation and can be formed by well-established lipid self-assembly protocols of general utility. Future work to control the number of vesicles on each nanodisk would be advantageous in order to achieve single vesicle level measurements.

Lastly, we wish to emphasize the sensing merits of LSPR in comparison to other label-free, surface-sensitive measurement techniques which are used to probe artificial lipid membranes and other biointerfacial systems. Nanoscale mass sensors are a common measurement approach, including optical-based techniques such as conventional surface plasmon resonance (SPR) and ellipsomtery and acoustic-based techniques such as quartz crystal microbalance (QCM). All of these techniques typically have penetration depths on the order of 100-nm or more, and the corresponding analysis models treat the adsorbate as a homogenous thin film. In contrast to these methodologies, LSPR sensing has up to an order-of-magnitude shorter penetration depth, thereby providing a highly surface-sensitive measurement that is influenced not only by lipid adsorption but also by membrane architecture (e.g., adsorbed vesicles versus planar lipid bilayer). Furthermore, LSPR sensing does not assume that the adsorbate constitutes a homogenous thin film, and is sensitive to the location where events occurs on the sensor substrate (i.e., proximity to deposited, plasmonic nanoparticles).

For these reasons, as control over the fabrication of plasmonic substrates continues to improve, LSPR-based methodologies may confer unique biosensing advantages that complement alternative surface-sensitive measurement strategies.

Experimental Section

Vesicle Preparation: Small unilamellar vesicles of 1-palmitoyl-2-oleoyl-*sn*-glycero-3-phosphocholine (POPC) (Avanti Polar Lipids, Alabaster, AL, USA) were prepared by the extrusion method using 30 nm track-etched polycarbonate membranes. The average diameter of extruded vesicles was below 60 nm.

LSPR Measurements: Optical extinction measurements were performed in transmission mode with the XNano instrument (Insplorion AB, Gothenburg, Sweden). For data acquisition and analysis, the Insplorer software (Insplorion AB) was used to determine the extinction maximum in the LSPR resonance spectrum by centroid calculation.[28] The coated sensor chips were obtained from Insplorion AB.

AFM Measurements: Contact mode imaging (~0.3 nN set point) was conducted using an NX-Bio microscope (Park Systems, Suwon, South Korea). A Biolever mini Si_3N_4 cantilever (Olympus, Tokyo, Japan) was used, with a nominal spring constant of 0.09 $N \cdot m^{-1}$ and a radius of curvature of ~8 nm.

Supporting Information

Supporting Information is available from the Wiley Online Library or from the author.

Acknowledgements

H. Z. Goh and J. A. Jackman contributed equally to this work. This work was supported by the National Research Foundation (NRF-NRFF2011–01) and the National Medical Research Council (NMRC/CBRG/0005/2012). J.A.J. is a recipient of the Nanyang President's Graduate Scholarship.

[1] K. A. Willets, R. P. Van Duyne, *Annu. Rev. Phys. Chem.* **2007**, *58*, 267–297.
[2] J. N. Anker, W. P Hall, O. Lyandres, N. C. Shah, J. Zhao, R. P. Van Duyne, *Nature Mater.* **2008**, *7*, 442–453.
[3] M. Estevez, M. A. Otte, B. Sepulveda, L. M. Lechuga, *Analyt. Chim. Acta* **2014**, *806*, 55–73.
[4] M. P. Jonsson, A. B. Dahlin, F. Höök, in *Nanoplasmonic Sensors* Springer, New York **2012**, pp. 59–82.
[5] A. B. Dahlin, N. J. Wittenberg, F. Höök, S.-H. Oh, *Nanophotonics* **2013**, *2*, 83–101.
[6] A. Dahlin, M. Zäch, T. Rindzevicius, M. Käll, D. S. Sutherland, F. Höök, *J. Am. Chem. Soc.* **2005**, *127*, 5043–5048.
[7] A. B. Dahlin, M. P. Jonsson, F. Höök, *Adv. Mater.* **2008**, *20*, 1436–1442.
[8] M. P. Jonsson, P. Jönsson, A. B. Dahlin, F. Höök, *Nano Lett.* **2007**, *7*, 3462–3468.
[9] M. P. Jonsson, P. Jönsson, F. Höök, *Analyt. Chem.* **2008**, *80*, 7988–7995.
[10] C. L. Baciu, J. Becker, A. Janshoff, C. Sönnichsen, *Nano Lett.* **2008**, *8*, 1724–1728.
[11] W. J. Galush, S. A. Shelby, M. J. Mulvihill, A. Tao, P. Yang, J. T. Groves, *Nano Lett.* **2009**, *9*, 2077–2082.
[12] H.-J. Wu, J. Henzie, W.-C. Lin, C. Rhodes, Z. Li, E. Sartorel, J. Thorner, P. Yang, J. T. Groves, *Nature Methods* **2012**, *9*, 1189–1191.
[13] E. M. Larsson, M. E. Edvardsson, C. Langhammer, I. Zoric, B. Kasemo, *Rev. Sci. Instruments* **2009**, *80*, 125105.
[14] J. Jose, L. R. Jordan, T. W. Johnson, S. H. Lee, N. J. Wittenberg, S. H. Oh, *Adv. Funct. Mater.* **2013**, *23*, 2785–2785.
[15] C. Keller, B. Kasemo, *Biophys. J.* **1998**, *75*, 1397–1402.
[16] I. Pfeiffer, B. Seantier, S. Petronis, D. Sutherland, B. Kasemo, M. Zäch, *J. Phys. Chem. B* **2008**, *112*, 5175–5181.
[17] C. Langhammer, E. M. Larsson, B. Kasemo, I. Zoric, *Nano Lett.* **2010**, *10*, 3529–3538.
[18] H. Fredriksson, Y. Alaverdyan, A. Dmitriev, C. Langhammer, D. S. Sutherland, M. Zäch, B. Kasemo, *Adv. Mater.* **2007**, *19*, 4297–4302.
[19] E. M. Larsson, C. Langhammer, I. Zorić, B. Kasemo, *Science* **2009**, *326*, 1091–1094.
[20] M. Schwind, S. Hosseinpour, C. Langhammer, I. Zorić, C. Leygraf, B. Kasemo, *J. Electrochem. Soc.* **2013**, *160*, C487–C492.
[21] N.-J. Cho, C. W. Frank, B. Kasemo, F. Höök, *Nature Protocols* **2010**, *5*, 1096–1106.
[22] R. C. MacDonald, R. I. MacDonald, B. P. M. Menco, K. Takeshita, N. K. Subbarao, L.-r. Hu, *Biochim. Biophys. Acta* **1991**, *1061*, 297–303.
[23] N.-J. Cho, S.-J. Cho, K. H. Cheong, J. S. Glenn, C. W. Frank, *J. Am. Chem. Soc.* **2007**, *129*, 10050–10051.
[24] N.-J. Cho, K. H. Cheong, C. Lee, C. W. Frank, J. S. Glenn, *J. Virology* **2007**, *81*, 6682–6689.
[25] L. Jiang, C. Zou, Z. Zhang, Y. Sun, Y. Jiang, W. Leow, B. Liedberg, S. Li, X. Chen, *Small* **2014**, *10*, 609–616.
[26] K. L. Young, M. B. Ross, M. G. Blaber, M. Rycenga, M. R. Jones, C. Zhang, A. J. Senesi, B. Lee, G. C. Schatz, C. A. Mirkin, *Adv. Mater.* **2014**, *26*, 653–659.
[27] K. Kumar, A. B. Dahlin, T. Sannomiya, S. Kaufmann, L. Isa, E. Reimhult, *Nano Lett.* **2013**, *13*, 6122–6129.
[28] A. B. Dahlin, J. O. Tegenfeldt, F. Höök, *Analyt. Chem.* **2006**, *78*, 4416–4423.

Received: February 25, 2014
Revised: June 21, 2014
Published online: July 30, 2014

